UCLA
UCLA Previously Published Works

Title
The effect of roughness elements on wind erosion: The importance of surface shear stress distribution

Permalink
https://escholarship.org/uc/item/7bj6k7z0

Journal
Journal of Geophysical Research: Atmospheres, 119(10)

ISSN
2169-897X

Authors
Webb, Nicholas P
Okin, Gregory S
Brown, Shannon

Publication Date
2014-05-27

DOI
10.1002/2014jd021491

Peer reviewed

eScholarship.org Powered by the California Digital Library
University of California

AGU PUBLICATIONS

JGR

Journal of Geophysical Research: Atmospheres

RESEARCH ARTICLE

10.1002/2014JD021491

Key Points:
- Roughness configuration has a significant effect on aeolian sediment flux
- Drag partition is sensitive to configuration but not captured in models
- Drag partition approaches overestimate flux by up to 3 orders of magnitude

Supporting Information:
- Readme
- Table S1
- Table S2
- Table S3
- Table S4

Correspondence to:
N. P. Webb,
nwebb@nmsu.edu

Citation:
Webb, N. P., G. S. Okin, and S. Brown (2014), The effect of roughness elements on wind erosion: The importance of surface shear stress distribution, *J. Geophys. Res. Atmos.*, *119*, 6066–6084, doi:10.1002/2014JD021491.

Received 15 JAN 2014
Accepted 31 MAR 2014
Accepted article online 3 APR 2014
Published online 28 MAY 2014

The effect of roughness elements on wind erosion: The importance of surface shear stress distribution

Nicholas P. Webb[1], Gregory S. Okin[2], and Shannon Brown[3]

[1]USDA-ARS Jornada Experimental Range, MSC 3 JER, NMSU, Las Cruces, NM, USA, [2]Department of Geography, University of California, Los Angeles, California, USA, [3]School of Environmental Sciences, University of Guelph, Guelph, Ontario, Canada

Abstract Representation of surface roughness effects on aeolian sediment transport is a key source of uncertainty in wind erosion models. Drag partitioning schemes are used to account for roughness by scaling the soil entrainment threshold by the ratio of shear stress on roughness elements to that on the vegetated land surface. This approach does not explicitly account for the effects of roughness configuration, which may be important for sediment flux. Here we investigate the significance of roughness configuration for aeolian sediment transport, the ability of drag partitioning approaches to represent roughness configuration effects, and the implications for model accuracy. We use wind tunnel measurements of surface shear stress distributions to calculate sediment flux for a suite of roughness configurations, roughness densities, and wind velocities. Roughness configuration has a significant effect on sediment flux, influencing estimates by more than 1 order of magnitude. Measured and modeled drag partitioning approaches overestimate the predicted flux by 2 to 3 orders of magnitude. The drag partition is sensitive to roughness configuration, but current models cannot effectively represent this sensitivity. The effectiveness of drag partitioning approaches is also affected by estimates of the aerodynamic roughness height used to calculate wind shear velocity. Unless the roughness height is consistent with the drag partition, resulting fluxes can show physically implausible patterns. These results should make us question current assessments of the magnitude of vegetated dryland dust emissions. Representing roughness effects on surface shear stress distributions will reduce uncertainty in quantifying wind erosion, enabling better assessment of its impacts and management solutions.

1. Introduction

Dust emissions produced by wind erosion in dryland environments are important for many Earth-system processes [*Ravi et al.*, 2011; *Shao et al.*, 2011]. Numerous models have been developed to evaluate rates of wind erosion and mineral dust emission [*Darmenova et al.*, 2009]. However, capturing the effects of soil and vegetation properties on dust emission remains a considerable and ongoing challenge. Increasing levels of model precision have not always improved accuracy in estimates of the frequency and magnitude of dust events or of the distribution of dust source areas in space and time [*Webb and McGowan*, 2009]. Accounting for surface roughness (vegetation) effects on aeolian transport is a key component of the model uncertainty [*Raupach and Lu*, 2004]. Reducing this uncertainty requires an understanding of how heterogeneous patterns of vegetation influence aeolian transport, and new insights into how near-surface aerodynamics moderated by vegetation can be captured in numerical modeling systems.

Aeolian sediment transport depends on aerodynamics close to the soil surface. The convention is to estimate horizontal sediment flux (Q) as a function of the wind shear velocity (u_*) incident on the land surface and in excess of a threshold shear velocity (u_{*t}) for particle entrainment [e.g., *Gillette and Passi*, 1988; *Sorensen*, 1991; *Shao et al.*, 1993]. The prevailing paradigm for implementing the aeolian transport model considers u_* to be related to the wind speed (U_z) at height z (m) and the aerodynamic roughness height (z_0) through the relationship described as the "Law of the Wall" [*Panofsky and Dutton*, 1984]. The threshold shear velocity (u_{*t}) for particle entrainment is used to describe the land surface threshold, accounting for both soil and vegetation components [e.g., *Shao et al.*, 1994; *Marticorena and Bergametti*, 1995].

Drag partitioning is typically used to represent surface roughness effects on wind erosion. The approach follows the hypothesis that "the main dynamical effect of adding roughness to an erodible surface is to increase u_{*t}" [*Raupach et al.*, 1993, 3023]. Here the threshold shear velocity of the soil is scaled by the ratio (R)

©2014. American Geophysical Union. All Rights Reserved.

of shear stress on the exposed soil surface to the total shear stress in the presence of roughness elements. For example [after *Shao*, 2008],

$$u_{*_t}(D, w, \lambda) = \frac{u_{*_{ts}}(D)}{R(z_0, \lambda)} H(w), \tag{1}$$

where $u_{*ts}(D)$ is the threshold shear velocity of the bare soil as a function of grain size, $H(w)$ is a correction function for soil moisture, and $R(z_0,\lambda)$ is the drag partition correction that is calculated as a function of the roughness height z_0 [*Marticorena and Bergametti*, 1995] or roughness density λ [*Raupach et al*., 1993]. Roughness density is the frontal area of roughness elements multiplied by their number density [*Marshall*, 1971]. The parameter is not sensitive to the distribution of roughness elements but varies with the spatial length scale (i.e., area) over which it is calculated and so is scale dependent.

Raupach et al. [1993] developed a drag partitioning model [after *Raupach*, 1992] with a scaling parameter ($m \leq 1$) to account for the nonuniformity in surface shear stress due to heterogeneous vegetation distributions. The m parameter scales λ to provide an estimate of the largest (i.e., maximum) shear stress ratio at the soil surface

$$R'' = \left[\frac{\tau''_S}{\tau}\right]^{1/2} = \left[\frac{1}{(1 - m\sigma_r\lambda)(1 + m\beta_r\lambda)}\right]^{1/2}, \tag{2}$$

where R'' is the maximum shear stress ratio, τ''_S is the maximum shear stress at the soil surface, τ is the total shear stress on the surface in the presence of roughness, β_r is the ratio of the drag coefficient for isolated roughness elements over the drag coefficient for the surface, and σ_r is the basal-to-frontal area ratio of the roughness elements [*Raupach et al*., 1993].

Field and laboratory wind tunnel studies suggest that the *Raupach et al*. [1993] model can provide a good approximation of the drag partition [*Marshall*, 1972; *Gillette and Stockton*, 1989; *Wolfe and Nickling*, 1996; *Lancaster and Baas*, 1998; *Gillies et al*., 2000, 2007; *Crawley and Nickling*, 2003; *King et al*., 2006]. However, a limitation to this approach, including *Marticorena and Bergametti* [1995] and *Walter et al*. [2012a], is that they estimate the *bulk* partition of shear stress between roughness elements and the exposed soil surface. The models omit the effects of roughness configuration on the distribution of surface shear stress and predict erosion across an entire model grid cell when $u_* > u_{*t}$. The bulk drag partitioning approach to scaling u_{*t} does not capture how the maximum shear stress can exceed the threshold for entrainment at one or a series of points in space, while the rest of the landscape remains inactive and does not produce saltation flux or dust emission. The approach does not explain well the observed heterogeneity in dust source activity or the timing and intensity of saltation and dust emission [*Gillette*, 1999; *Okin and Gillette*, 2001; *Li et al*., 2013].

An alternative conceptualisation of aeolian transport is to consider u_{*t} to be a property describing the soil surface erodibility (u_{*ts}) alone. The threshold is independent of vegetation roughness, which affects the wind erosivity (u_*). Thus, drag partitioning between roughness elements and the soil surface affects the distribution of surface shear stress (τ_S) that can act on the area of exposed soil surface [*Okin*, 2008]. The distribution of τ_S is directly related to the freestream wind velocity and the distribution of roughness elements with respect to the direction from which the wind is blowing [*Gillette et al*., 2006]. This approach considers where and when u_* exceeds u_{*t} to induce sediment flux within a landscape. It does not rely on spatial averages or maxima to describe the effect of vegetation on saltation flux and dust emission.

Okin [2008] presented a wind erosion model which makes explicit roughness distribution effects on τ_S. The approach is supported by *Walter et al*. [2012b] who show that the magnitude of τ_S varies locally around roughness elements and can have a significant effect on sediment flux. *Li et al*. [2013] demonstrated that accounting for vegetation distribution more accurately predicts saltation flux than models based on bulk drag partitioning [e.g., *Raupach et al*., 1993; *Marticorena and Bergametti*, 1995]. Their research also indicated that the approach may better capture the frequency of saltation events by enabling u_* to exceed u_{*t} within large canopy interspaces that may be present even at high-fractional cover levels. Uncertainty in aeolian sediment transport models may be significantly reduced by accounting for the distribution of roughness elements. However, only recently has the effect of τ_S distributions on sediment flux been the subject of investigation [e.g., *Walter et al*., 2012b; *Dupont et al*., 2014].

©2014. American Geophysical Union. All Rights Reserved.

Brown et al. [2008] measured spatially and temporally the average surface shear stress (τ'_S) and total shear stress (τ) for a range of roughness configurations ("staggered," "random," "clumped," and "streets"), roughness densities (λ), and freestream wind velocities (U_f). Analyzed in the context of the *Raupach et al*. [1993] model, *Brown et al*. [2008] concluded that roughness configuration has only a small impact on the average (R) and maximum (R'') drag partition. Descriptive statistics (mean, standard deviation, and skewness) for the τ'_S distributions did not reveal significant differences between roughness configurations. Surface protection was found to increase with increasing λ but appeared to be independent of roughness configuration under the bulk drag partitioning model.

The *Raupach et al*. [1993] approach only approximates well measurements of R'' when critical model parameters β_r and m are measured and calculated relative to R'' [*Brown et al*., 2008]. This reveals a further weakness of this model, that β_r and m are dependent on U_f, λ and roughness element shape. Similarly, the *Raupach et al*. [1993] model does not work well for different roughness configurations unless the β_r parameter values, which by definition should be constant among configurations, are made variable [*Crawley and Nickling*, 2003; *Walter et al*., 2012a]. While the *Brown et al*. [2008] study demonstrated the utility and limitations of bulk drag partitioning approaches, such data have not been applied to assess the significance of roughness configuration for sediment flux, or how effective alternative approaches can be for improving on the current modeling paradigm.

The objectives of this paper are to (1) numerically test the hypothesis that the spatial configuration of roughness elements has a significant effect on horizontal aeolian sediment flux (Q) and (2) evaluate the ability of the bulk drag partitioning approach to represent roughness configuration effects on Q. We conduct the assessment by using data from *Brown et al*. [2008] to evaluate the sensitivity of Q to differences in measured surface shear stress distributions for four roughness configurations. We compare the flux estimates with those derived from measured and modeled drag partitions (R''), accounting for different levels of variability in model input parameters that represent roughness effects on u_* and u_{*t}. We then use the analysis to draw conclusions about the importance of roughness configuration for sediment flux and the implications of the two conceptual approaches for modeling wind erosion.

2. Methods

2.1. Available Data

Data from *Brown et al*. [2008] provided a basis for our examination of the effects of roughness configuration on Q. We provide an overview of their methodology here. The objective of *Brown et al*. [2008] was to assess the effect of roughness configuration on the average drag partition and shear stress ratio, including estimates of R and R'' using the *Raupach et al*. [1993] model. The study thus developed a data set with measurements of τ, τ'_S, τ''_S, u_*, and z_0 for a range of roughness densities and configurations.

The recirculating wind tunnel at the Wind Erosion Laboratory, University of Guelph, was used for all roughness measurements [*Brown et al*., 2008]. The wind tunnel has a working section that is 8.0 m long, 0.72 m high, and 0.92 m wide. Film canisters filled with cement acted as roughness elements (height (h) = 4.9 cm, diameter (d) = 3.1 cm, σ = 0.50). Stress measurements were made for four different roughness configurations: staggered, random, clumped, and streets [after *Okin and Gillette*, 2001]. The staggered array was included as it is commonly used in wind tunnel studies [e.g., *Crawley and Nickling*, 2003; *King et al*., 2006], while the remaining configurations were chosen to represent natural arrays of vegetation. Each configuration was examined at four roughness densities, λ = 0.02, 0.0342, 0.0585, and 0.11.

Each configuration and density combination was subject to five freestream wind velocities, U_f = 6.58, 8.71, 10.92, 12.92, and 14.87 m s^{-1}. A pitot tube connected to a ThermoBrandt 12.7 mm (0.5 inch) differential pressure transducer (ThermoBrandt Ltd.) was placed 6.94 m downwind of the start of the working section of the wind tunnel to measure the wind speed profile at 14 heights. The wind speed profiles were used to calculate z_0 and u_* using the logarithmic wind profile equation, the Law of the Wall [*Panofsky and Dutton*, 1984].

A tiered force balance was used to measure τ_R. Two drag plates were used to independently measure the drag on the surface (τ_S) and the roughness elements (τ_R). These are related to the total drag on the rough surface (τ) through the expression: $\tau = \tau_S + \tau_R + \tau_C$, where τ_C is the roughness element surface drag due to skin

©2014. American Geophysical Union. All Rights Reserved.

friction of the roughness elements. The τ_C was neglected here due to the small evaluated λ [*Shao and Yang*, 2008]. Each plate measured stress with a Surface Mount Technology (SMT) Interface force transducer placed between a free-moving arm and a fixed metal cylinder. The transducers were attached to separated aluminum frames that held plywood sheets (0.6 m wide by 1.8 m long). Roughness elements "floated" on the surface plate and were connected to the lower roughness plate via metal rods to allow for the independent and simultaneous measurements. The tiered force balance was located in a 0.625 m × 1.080 m opening in the wind tunnel floor, 5.9 m downwind in the working section. A data logger was used to record the output of the force transducers at 10 Hz.

Irwin sensors [*Irwin*, 1980] embedded in the surface of the force balance plate were used to make point measurements of τ_S within the roughness arrays. This enabled an examination of the spatial distribution of maximum (τ''_S) and average (τ'_S) surface shear stress. The Irwin sensors measure skin friction using a pressure transducer (ThermoBrandt Ltd., 12 mm differential pressure transducer; Model DPT 32S12-0.5; precision ± 0.25% full scale) attached to a 12.5 mm diameter brass cylinder with two openings: one 2.57 mm diameter center tap for a surface pressure port and a second port within the center tap consisting of a 16-gauge stainless steel tube extending 1.75 mm above the surface. Output from the pressure transducer was recorded by a data logger. The design enabled detection of the near-surface pressure differential at a frequency of 10 Hz.

For the staggered arrays, Irwin sensors were placed in a grid pattern between roughness elements similar to *Crawley and Nickling* [2003]. Using this pattern resulted in close agreement between τ'_S measured by the force balance and τ'_S measured by the Irwin sensors. For the remaining roughness configurations, the Irwin sensors were positioned to cover a range of relatively more open areas and areas in the lee of the roughness elements. The maximum stress on the surface (τ''_S), combined with the τ from the force balance, provided a direct estimate of R'' as $(\tau''_S/\tau)^{0.5}$ (equation (2)).

The theory of *Raupach et al*. [1993] suggests that R'' can also be estimated from structural parameters (equation (2)) based on estimates of the values of β_r and m. The β_r parameter is calculated as the ratio of the drag coefficient of a roughness element (C_R) to the drag coefficient of the surface (C_S), each calculated as

$$C_R = \frac{\varphi}{\rho_a \mathrm{d} h U_h^2}, \text{and} \tag{3}$$

$$C_S = \frac{\tau_{S(\lambda=0)}}{\rho_a U_h^2}, \tag{4}$$

where ρ_a is air density (1.204 kg m^{-3}), U_h is the wind speed at the roughness element height, $\tau_{S(\lambda=0)}$ is the mean surface drag in the absence of roughness, and ϕ is the drag force on an individual roughness element [*Raupach et al*., 1993]. The surface drag plate with no roughness elements provided $\tau_{S\ (\lambda=0)}$. For C_R, ϕ was measured using a single element attached to the roughness plate. Measuring drag coefficients at each U_f resulted in values of β_r that ranged from 158 to 248 due to a dependency of β_r on U_f, which affects the drag force on roughness elements. The m parameter values were calculated for each array as the difference between the maximum and average surface shear stresses as measured by the Irwin sensors [*Luttmer*, 2002]:

$$m = 1 - \frac{\tau''_S - \tau'_S}{\tau''_S}. \tag{5}$$

Values of m calculated this way ranged from 0.33 to 0.63, with a mean of 0.49. The calculated m did not show significant differences between the different configurations but did show dependence upon λ and U_f. The latter finding is contrary to the original formulation of the m parameter by *Raupach et al*. [1993], which was thought to be a constant, suggesting a weakness in the theory. That the use of average (constant) values of m will result in significant errors in estimates of R'' using the *Raupach et al*. [1993] theory (equation (2)) is further testament to this fact [*Brown et al*., 2008].

2.2. Data Analysis

Two approaches were taken to investigate the effects of roughness configuration and measured and modeled drag partitions on horizontal sediment flux Q: (1) the "τ'_S distribution method," wherein Q was calculated with u_* provided by the measured τ'_S distributions and (2) the "R'' method," wherein Q was calculated with u_{*t} estimated from measured and modeled bulk drag partitions (R'').

©2014. American Geophysical Union. All Rights Reserved.

2.2.1. The τ'_S Distribution Method

The objective of the τ'_S distribution method was to calculate Q as a function of the distribution of measured τ'_S, thus showing the absolute effect of roughness configuration on sediment flux. Here we converted each value of τ'_S in the measured distributions to a friction velocity (u_*) following *von Kármán* [1934]:

$$u_* = \sqrt{\frac{\tau'_s}{\rho_a}}. \tag{6}$$

The sediment flux Q for each measured τ'_S, for the respective combinations of roughness configuration, λ and U_f, was calculated for a nominal range of u_{*ts} = 0.25 m s^{-1} to 0.45 m s^{-1}; consistent with the entrainment threshold for erodible fine sands [*Gillette et al.*, 1980]. The estimates of Q were obtained using the *Shao et al.* [1993] flux equation:

$$Q = A\frac{\rho_a}{g}\Sigma_{u_*} u_* \left(u_*^2 - u_{*t}^2\right), \tag{7}$$

where Q is the horizontal sediment mass flux (g m^{-1} s^{-1}), A is a dimensionless parameter related to the supply limitation of soil grains, assumed here to be 0.54 [*Shao*, 2008], and g is the acceleration of gravity (9.81 m s^{-2}). As the roughness elements were assumed to affect u_* under this approach, u_{*t} was assigned the values of u_{*ts}. We selected the *Shao et al.* [1993] flux equation on the basis that it has been applied extensively with the *Raupach et al.* [1993] drag partitioning scheme [*Shao*, 2008]. However, the exact form of the equation is not important here. Most common flux equations are also threshold controlled, raise u_* to the second or third power [e.g., *Li et al.*, 2013], and will thus show similar patterns. The weighted average of Q for each τ'_S, for the combinations of roughness configuration, λ and U_f, was then calculated by

$$Q = (1 - F_c)\sum p(\tau'_s)Q\left(\tau'_s, u_{*_{ts}}\right), \tag{8}$$

where F_c is the surface fraction covered by roughness elements and $p(\tau'_S)$ is the probability of a measured τ'_S from the laboratory experiments. Equation (8) provides an estimate of the "transport limited" saltation, and we do not account here for the supply limitation of erodible sediment that occurs on natural surfaces or the effect of roughness element size (height and width) in reducing sediment transport efficiency [*Gillies and Lancaster*, 2012]. The model also does not account for equilibrium saltation. We assume this would not adversely affect the results under the patchy surface shear stress distributions evaluated here.

Using a range of u_{*ts} in the flux calculations provided a means for testing the sensitivity of Q to roughness configuration and U_f with respect to the threshold for soil particle entrainment. The relative effect of the roughness configurations was then determined by calculating the ratio of Q for the "nonstaggered" arrays (random, clumped, and streets) to the "staggered" arrays at corresponding λ and U_f. Comparisons were made with the staggered configuration as it has formed the basis of preceding analyses of roughness effects on drag partition [e.g., *Marshall*, 1971; *Dong et al.*, 2001; *Crawley and Nickling*, 2003]. This approach enabled a comparison of the absolute and relative effects of roughness configuration on sediment flux.

To determine how differences in the shape of the u_* histogram might affect relative rates of Q under wind speeds that might be experienced by a real site over a period of time, we calculated the ratio of Q between the streets and random configurations. We used τ measurements to estimate u_* ($\tau = \rho\, u_*^2$) for both configurations (λ = 0.11) for the five U_f used in the wind tunnel experiments (6.59, 8.71, 10.92, 12.92, and 14.87 m s^{-1}) [*Brown et al.*, 2008]. Each of the values of τ is related to a histogram of τ_s from the Irwin sensors. In order to estimate the histogram of τ_s that would have been measured by the Irwin sensors for wind speeds not run in the wind tunnel, we interpolated the histogram. This was done by interpolating between measured probabilities within each τ_s bin using a spline, then normalizing the resultant interpolated histograms to ensure that the new probability distributions created through this process summed to one. A theoretical Weibull distribution of u_*, with shape parameter equal to 3.87 and scale parameter equal to 0.77 m s^{-1}, was estimated from long-term wind speed measurements at 15 m height in the Jornada Basin in south central New Mexico, USA. Total flux for each u_* bin in the theoretical Weibull-derived u_* distribution was calculated as the sum of Q calculated (using equation (7)) for each τ_s bin

©2014. American Geophysical Union. All Rights Reserved.

multiplied by the probability of that τ_s occurring (i.e., the τ'_S distribution method). Total flux for each configuration (streets and random) was then calculated as the sum of the resulting Q multiplied by the probability of the specific u_* occurring within the theoretical Weibull-derived u_* distribution.

2.2.2. The R″ Method

The objectives of the R'' method were to (1) evaluate the ability of the drag partitioning approach to represent the predicted roughness configuration effects on Q (section 2.2.1) and (2) compare measured and modeled [after *Raupach et al*., 1993] drag partitioning effects on Q to identify sensitivities of the bulk drag partitioning approach that influence its performance. Here, we calculated the land surface threshold friction velocity u_{*t} after *Shao* [2008], following directly from the definition of R'' in *Raupach et al*. [1993]:

$$u_{*_t}\left(u_{*_{ts}},\lambda\right) = \frac{u_{*_{ts}}}{R''}, \tag{9}$$

where u_{*t} is the bare soil threshold friction velocity scaled by the measured or modeled [*Raupach et al*., 1993] maximum drag partition. We again used a nominal range of $u_{*ts} = 0.25$ m s^{-1} to 0.45 m s^{-1} to initiate the flux calculations. Four approaches were evaluated for their ability to represent surface roughness effects on R'', u_*, and estimates of Q calculated using equation (7). Each test of the effect of measured and modeled R'' on Q provided insights into the capability of the *Raupach et al*. [1993] model to capture the effects of the drag partition and roughness configuration on Q.

First, we calculated Q using the measured R'' (Table S1 in the supporting information) and R'' modeled after *Raupach et al*. [1993] (equation (2)) with measured β_r and calculated m parameters for the range of roughness configurations, λ and U_f (Table S2) [*Brown et al*., 2008]. For both calculations the shear velocity (u_*) was estimated from the wind tunnel experiments for each corresponding roughness configuration, λ and U_f following a reorganization of the Law of the Wall [*Panofsky and Dutton*, 1984]:

$$u_* = \frac{U_z k}{ln(z/z_o)}, \tag{10}$$

where U_z is the wind speed at height, z, k is the von Kármán constant (~0.4), and z_o is the aerodynamic roughness height. U_z was taken as the freestream wind velocity in the wind tunnel (U_f) and z as the height above the wind tunnel bed where this speed was measured (0.37 m). The roughness height z_0 was derived from wind speed profile data (section 2.1) for each wind tunnel experiment [*Brown et al*., 2008]. Values of the estimated z_0 and u_* derived from the wind tunnel measurements are provided in Tables S3 and S4, respectively. Comparing the estimates of Q calculated from the measured and modeled R'' enabled direct assessment of the ability of the *Raupach et al*. [1993] model, with input parameters specific to each roughness configuration, to represent the configuration effects on Q.

The approach of predicting Q using measured u_* revealed a sensitivity of Q to estimates of u_* derived from the measured z_0. To evaluate the effect of this sensitivity further, we calculated Q as product of the measured and modeled R'' while holding z_0 constant at 4.0×10^{-3} m for all roughness configurations and λ. This nominal value of z_0 represents the mean of the measured z_0 for all roughness configurations, λ and U_f, in the wind tunnel experiments [*Brown et al*., 2008]. Using a constant z_0 had the effect of removing localized roughness element wake influences on u_* and Q.

Thirdly, we reintroduced variability in z_0 by estimating the parameter as a function of λ, following *Marticorena et al*. [1997] and *Marticorena et al*. [2006]:

$$\text{for}\,\lambda < 0.045 \quad \log(z_0/h) = 1.31(\log(\lambda)) + 0.66, \text{ and} \tag{11}$$

$$\text{for}\,\lambda \geq 0.045 \quad \log(z_0/h) = -1.16, \tag{12}$$

where h is the geometrical height of the roughness elements. We thus calculated Q for each roughness configuration, λ and U_f, using the measured and modeled R'' and u_* values derived from z_0 following equations (11) and (12). The derived values of z_0 were of a similar order of magnitude to the measured values (Table S3) but did not vary among the roughness configurations: 5.7×10^{-4} m ($\lambda = 0.02$), 1.2×10^{-3} m ($\lambda = 0.0342$), 1.55×10^{-2} m ($\lambda = 0.0585, 0.11$). This approach enabled us to account for the effect of

©2014. American Geophysical Union. All Rights Reserved.

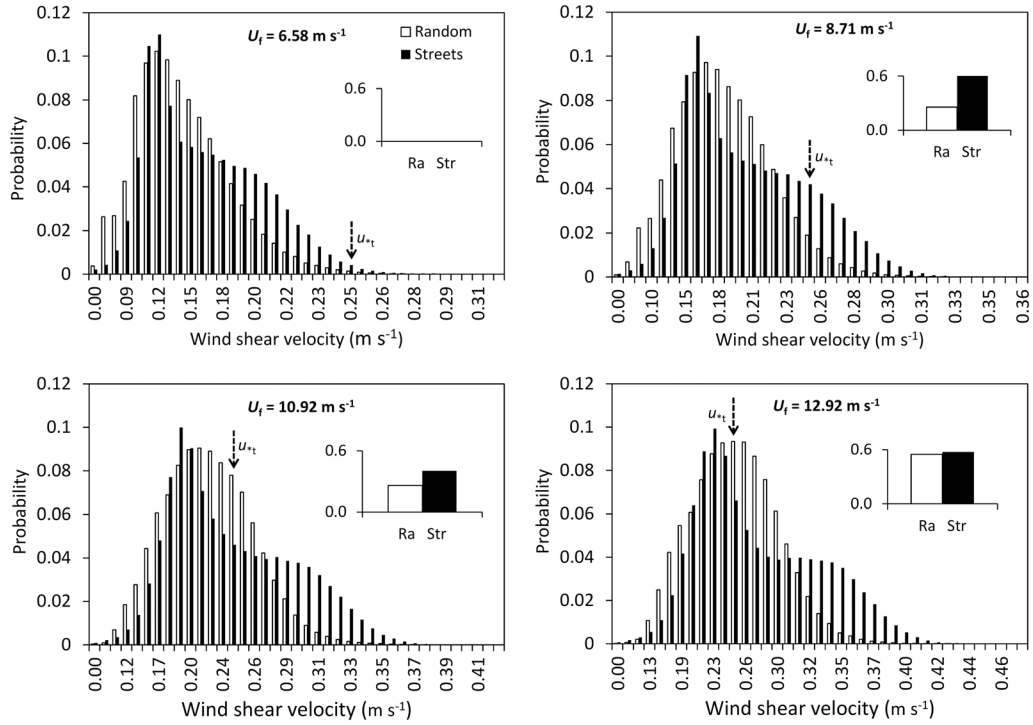

Figure 1. Histograms illustrating the effect of the random and street roughness configurations on wind shear velocity (u_*) calculated from measured surface shear stress (τ'_S) distributions at a roughness density (λ) of 0.10 and four freestream wind velocities (U_f). Inset graphs show the proportion of τ_S greater than a nominal threshold shear velocity (u_{*t}) of 0.25 m s^{-1} for the random (Ra) and street (Str) configurations.

λ on z_0, while removing other sources of variability in z_0 that could be a product of roughness element position with respect to the pitot tubes for measuring U_f, and roughness configuration.

Finally, we evaluated the effect on Q of holding the m and β_r parameters constant to estimate R'', following the implementation of the *Raupach et al.* [1993] scheme by *Shao et al.* [1994]. Values for m (0.49) and β_r (200) were taken as the average of those measured by *Brown et al.* [2008] across the roughness configurations. The calculated R'' and values of u_* derived from λ (equations (11) and (12)) were then used to estimate Q for each roughness configuration, λ and U_f.

3. Results

3.1. The Effect of Roughness Configuration on Flux

The effect of roughness configuration on the distribution of measured surface shear stress, expressed as u_*, is illustrated in Figure 1. The distribution and proportion of τ'_S, and therefore u_*, varies between roughness configurations at a constant λ under the four measured U_f. There is considerable overlap in the τ_S distributions for the roughness configurations. There are also significant differences in the distribution of τ'_S relative to the soil threshold for entrainment. This is expressed as differences in the shape (modality) of the u_* distributions. The data suggest that roughness configuration can affect the proportion of a land surface over which u_* exceeds u_{*t} and is therefore likely important for horizontal sediment flux (Q) and dust emission.

As a first approximation of the significance of roughness configuration for Q we calculated the proportion of τ'_S in excess of an arbitrary threshold for soil particle entrainment, u_{*ts} = 0.25 m s^{-1} (Table 1). The proportion of τ'_S in excess of the threshold clearly increases with increasing U_f and is greater for small roughness densities than for large roughness densities. At low U_f and large λ, and at high U_f at small λ, the proportion of τ'_S in excess of the threshold is similar among the roughness configurations. This indicates

©2014. American Geophysical Union. All Rights Reserved.

Table 1. Proportion of the Surface Shear Stress (τ'_s) Distributions Exceeding an Arbitrary Threshold for Transport, Set to τ_S = 0.15 N m^{-2} (Equivalent to u_* = 0.25 m s^{-1} for Sandy Soils)[a]

		Proportion of τ'_s Distribution > u_{*t} = 0.25 m s^{-1}				
Roughness Configuration	λ	U_f = 6.58	U_f = 8.71	U_f = 10.92	U_f = 12.92	U_f = 14.87
Staggered	0.02	0.16	0.77	0.86	0.96	0.99
Clumped		0.28	0.66	0.77	0.88	0.96
Random		0.12	0.59	0.75	0.93	0.99
Streets		0.17	0.71	0.90	0.95	1.00
Staggered	0.0342	0.03	0.44	0.79	0.93	0.98
Clumped		0.07	0.44	0.64	0.80	0.88
Random		0.06	0.47	0.75	0.87	0.91
Streets		0.05	0.49	0.78	0.90	0.96
Staggered	0.0585	0.01	0.22	0.61	0.85	0.94
Clumped		0.02	0.34	0.74	0.87	0.93
Random		0.01	0.23	0.65	0.82	0.90
Streets		0.02	0.37	0.67	0.84	0.92
Staggered	0.11	0.00	0.06	0.27	0.55	0.72
Clumped		0.00	0.09	0.41	0.62	0.76
Random		0.00	0.04	0.26	0.55	0.75
Streets		0.01	0.16	0.40	0.58	0.80

[a]Data are shown for the set of four roughness configurations at a range of roughness densities (λ) and freestream wind velocities (U_f) (m s^{-1}).

that roughness configuration may have little effect on sediment flux under these conditions because either none or all of the τ'_S is above the entrainment threshold. Between these extremes roughness configuration can have a large effect on the proportion of τ'_S in excess of the threshold (Table 1). The magnitude of the difference in excess τ'_S varies between roughness configurations and with U_f. This suggests that the significance of roughness configuration for Q is dependent on the proximity of u_* to u_{*t} over the land surface.

Calculating sediment flux from the measured τ'_S distributions reveals that roughness configuration has a significant effect on estimated sediment flux (Figure 2). There is a consistent pattern in Q across the roughness configurations, λ and U_f. The modeled sediment flux increases with decreasing λ and an increase in U_f. Sediment flux appears to be most sensitive to roughness configuration at small λ and low U_f (large differences in Q between configurations), and least sensitive to roughness configuration at large λ and U_f (small or no difference in Q). Differences in Q between the configurations get smaller with increasing U_f. However, Q for the clumped and streets configurations and the staggered and random configurations show similar response patterns to changes in λ. This suggests that the pairs of roughness configurations may induce similar patterns in the probability distribution of τ'_S, which are reflected in the calculated Q.

The relative effect of the measured roughness configurations (staggered, clumped, random, and streets) on sediment flux is shown in Figure 3. Roughness configuration is most important for Q at low U_f, at large λ, and as u_* approaches u_{*t}. For u_{*t} = 0.25 m s^{-1} at the lowest shown U_f (8.71 m s^{-1}), the modeled Q at the largest roughness density (λ = 0.11) is nearly 3 times the magnitude of Q at the smallest λ (0.02). As U_f increases toward 14.87 m s^{-1} the effect of roughness configuration on Q declines. The modeled sediment flux for nonstaggered arrays was found to be nearly 2 times larger than for the staggered arrays (λ = 0.11) , but there is little difference at the smallest roughness densities (λ = 0.02, 0.0342).

As u_* approaches u_{*t} = 0.35 m s^{-1} the magnitude of the difference in modeled Q for the nonstaggered relative to staggered roughness configurations increases (Figure 3). For example, modeled Q for the streets configuration is 16 times larger than for the staggered configuration at U_f = 12.92 m s^{-1}, and 10 times larger at U_f = 14.87 m s^{-1}. We found the streets roughness configuration to have consistently larger modeled Q than the clumped and random configurations, particularly at the larger measured roughness density (λ = 0.11). At u_{*t} = 0.425 m s^{-1} our results show that no sediment flux would be initiated under freestream wind velocities of 8.71 m s^{-1} and 10.92 m s^{-1}. This is because the distribution of τ'_S was below the nominal soil

©2014. American Geophysical Union. All Rights Reserved.

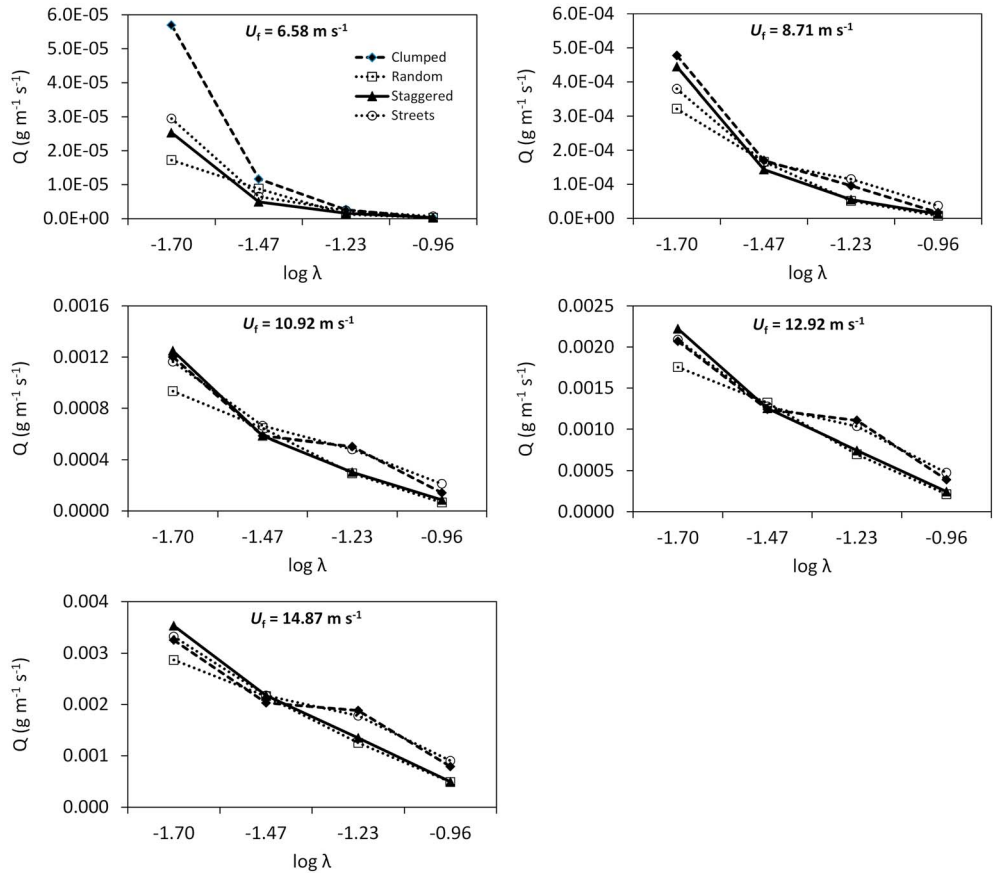

Figure 2. Plots of horizontal sediment mass flux Q (g m^{-1} s^{-1}) calculated from the τ_s distribution method versus $\log_{10}(\lambda)$ for the set of four roughness configurations at a range of λ and freestream wind velocities (U_f). Initial u_{*t} set to 0.25 m s^{-1}.

threshold for entrainment. The magnitude of the difference in modeled Q between roughness configurations declines at small λ, but at the largest measured λ (0.10) and U_f (12.92 and 14.87 m s^{-1}) modeled Q for the streets and clumped roughness configurations were 10 to 20 times that of the staggered configuration (Figure 3).

The ratio of estimated Q for the streets configuration to the estimated Q for the random configuration using a theoretical Weibull distribution of wind speed was never less than two (Figure 4). The ratio reached a maximum of 19 at u_{*t} = 0.37 m s^{-1} and was greater than five for $u_{*t} \geq 0.27$ m s^{-1}. These results indicate that, even under conditions of variable wind speed, roughness configuration can likely have a large effect on aeolian sediment transport. The peak of this influence at u_{*t} = 0.37 m s^{-1} results from the major differences between the histogram of shear velocity starting ~0.37 m s^{-1} at high wind speeds (Figure 1).

3.2. Estimating Flux From the Drag Partition

Comparing the ratio of measured R'' for the staggered and nonstaggered arrays reveals the sensitivity of the maximum shear stress ratio to roughness configuration (Figure 5). The data show that there is very little difference in R'' between the nonstaggered configurations, or between the nonstaggered and staggered configurations, except at low roughness densities (λ = 0.02). These differences in R'' between the staggered and nonstaggered configurations at λ = 0.02 are reduced as U_f increases from 6.85 m s^{-1} and 14.87 m s^{-1}. This suggests that the modeled sediment flux with u_{*t} adjusted by R'' (i.e., the R'' method) may be similar at large roughness densities. At small roughness densities (e.g., λ = 0.02), the effect of differences in R'' on Q due to roughness configuration could be significant.

Indeed, estimates of sediment flux based on the measured maximum surface shear stress (τ''_S) confirm that Q predicted from R'' ($(\tau''_S/\tau)^{0.5}$) should be somewhat sensitive to roughness configuration (Figure 6). As for

©2014. American Geophysical Union. All Rights Reserved.

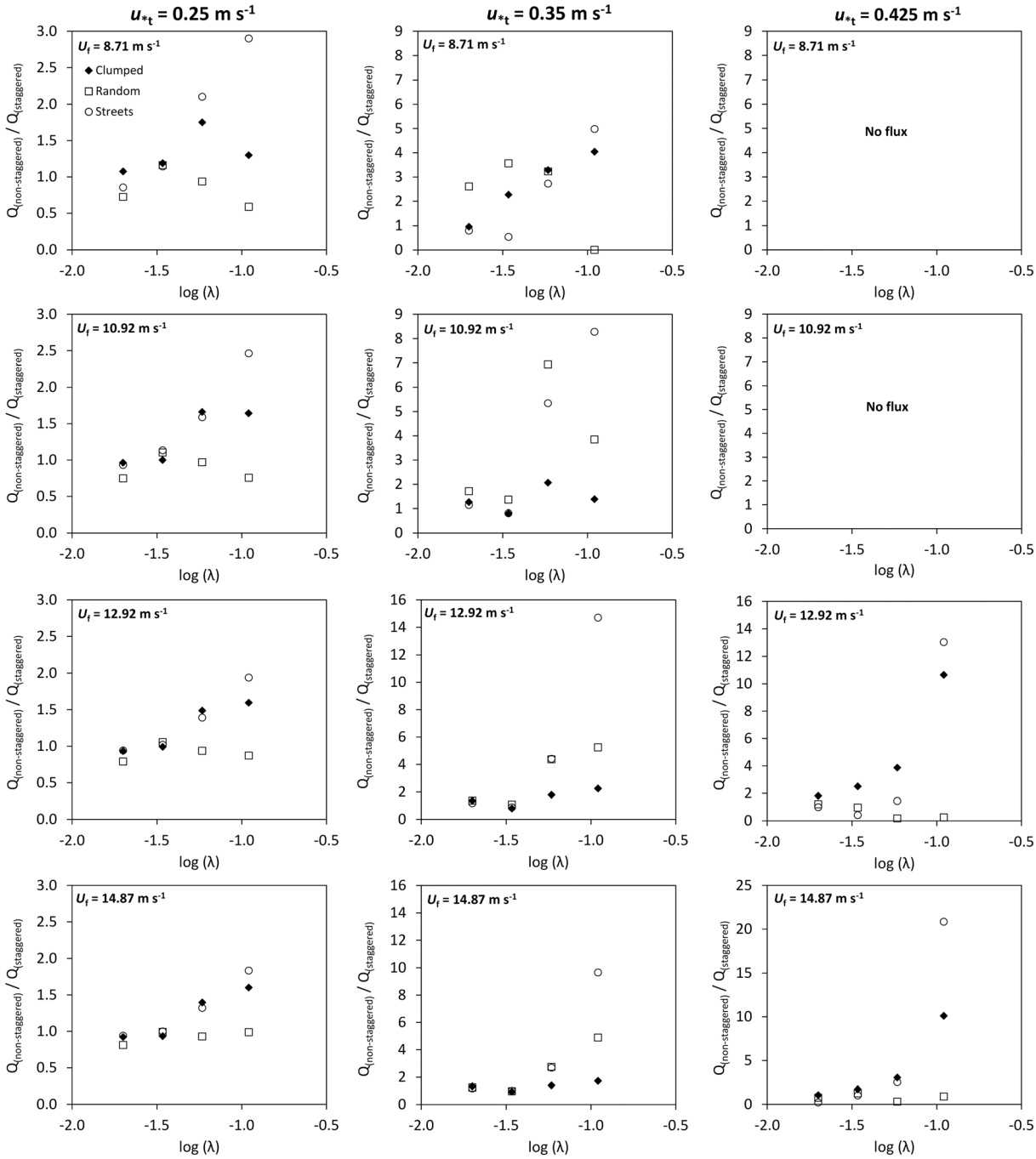

Figure 3. Graphs showing the effect of roughness configuration on horizontal sediment mass flux (Q), expressed as the ratio of Q for the clumped, random, and street configurations relative to Q for the staggered configurations at a range of roughness densities (λ) and freestream wind velocities (U_f).

estimates of Q based on the measured τ'_S distributions, differences in Q among the roughness configurations are largest at small λ and small U_f, while Q declines with increasing λ for all configurations. Importantly, the estimates of Q based on the measured τ''_S are between 1 and 3 orders of magnitude larger than those based on the τ'_S distribution method. This was expected because flux estimates derived from the R'' method assume that flux is initiated uniformly in space, so Q is likely to be significantly larger than when accounting for the distribution of surface shear stress.

©2014. American Geophysical Union. All Rights Reserved.

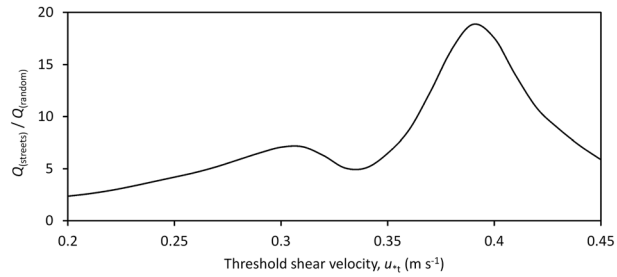

Figure 4. Graph showing the ratio of horizontal sediment mass flux Q (g m^{-1} s^{-1}) for the streets configuration to Q for the random configuration (λ = 0.11) calculated from a theoretical Weibull distribution of u_* and plotted for a nominal range of threshold friction velocities (u_{*t}).

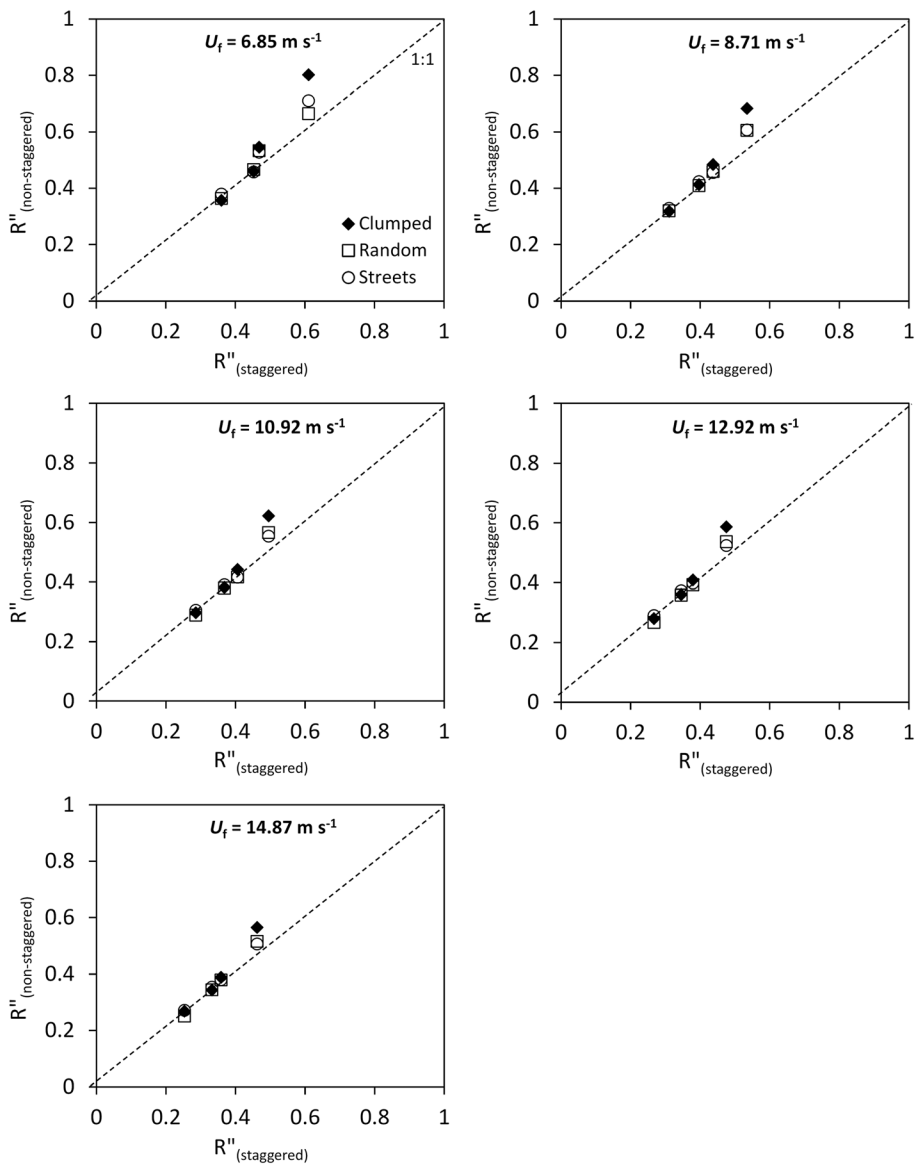

Figure 5. Plots of the measured maximum shear stress ratio (R'') for nonstaggered arrays against R'' for the staggered array for a set of freestream wind velocities (U_f).

©2014. American Geophysical Union. All Rights Reserved.

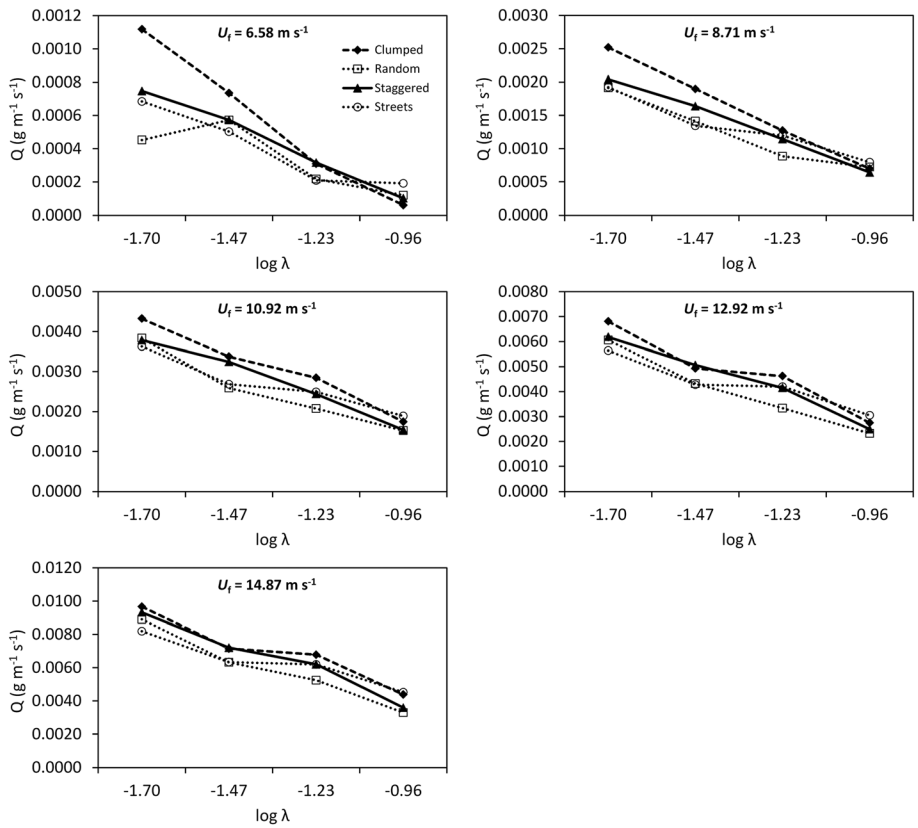

Figure 6. Graphs showing the effect of maximum shear stress (τ''_S) on Q for the set of four roughness configurations at a range of λ and freestream wind velocities (U_f). Initial u_{*t} set to 0.25 m s^{-1}.

Figure 7 compares values of Q calculated from the measured and modeled R'' and measured u_*. Q predicted by either approach displays an unexpected response pattern to changes in roughness density. Sediment flux both increases and decreases with increasing λ rather than declining at larger roughness densities (e.g., Figures 2 and 6). That the estimated values for Q are similar for the measured and modeled R'' indicate that the *Raupach et al*. [1993] model may reasonably represent the measured R'', as indicated by *Brown et al*. [2008]. However, the absence of a monotonic decrease in estimated Q with increasing λ indicated a problem with using the measured z_0 to predict u_* from the wind tunnel experiments.

Employing a constant z_0 to predict u_* resolved some of the unexpected behavior in the modeled Q response to increasing λ (Figure 8). Here, estimates of Q with both the measured and modeled R'' follow a pattern closer to that expected from field studies [*Lancaster and Baas*, 1998] and predicted from the τ'_S distributions (Figure 2). We believe that the difference between Q calculated with measured z_0 (Figure 7) and constant z_0 (Figure 8) results from z_0 (measured at a single point in the wind tunnel) being sensitive to both roughness configuration and density; measurements of U_f used to derive z_0 were likely affected by the placement of the pitot tubes with respect to the roughness elements during the wind tunnel experiments. That is, for some roughness configurations the pitot tube measurements (from the same position in the wind tunnel) were affected by the local depression of shear stress in the lee of adjacent roughness elements. For other configurations the pitot tube may not have had adjacent roughness elements and so was not affected by a local depression of shear stress.

To isolate the effect of roughness density from roughness configuration on estimates of z_0, we estimated flux using common means to estimate z_0 from λ. Figure 9 shows the response of Q to roughness configuration, U_f and λ, predicted from the measured and modeled R'' and z_0 derived following equations (11) and (12). The flux response is again unexpected, showing a pattern of increasing Q with increasing roughness density at high U_f. It does not follow our predicted flux behavior with respect to λ for the measured τ'_S distributions

©2014. American Geophysical Union. All Rights Reserved.

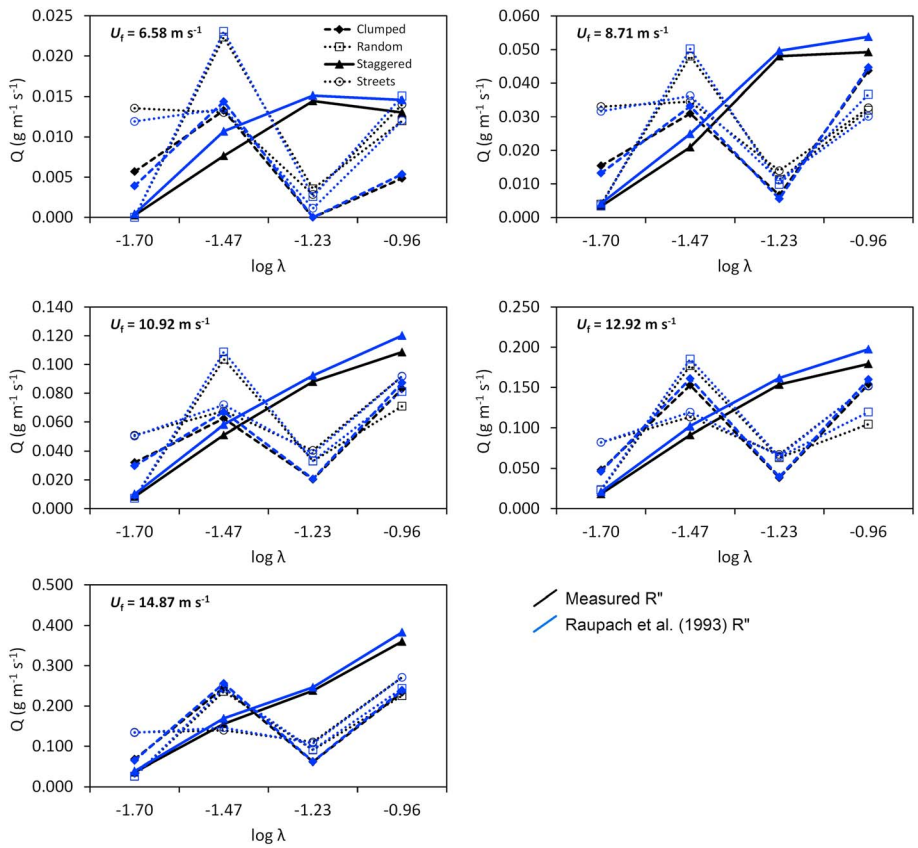

Figure 7. Plots of horizontal sediment mass flux Q (g m^{-1} s^{-1}) calculated from the measured and modeled [after *Raupach et al.*, 1993] R'' for the set of four roughness configurations at a range of λ and freestream wind velocities (U_f). Initial u_{*t} set to 0.25 m s^{-1}. Estimates of u_* as input to Q were based on measured z_0 in the wind tunnel experiments.

(Figure 2). Nor does this conform to observations from the field, which show that Q may decline by 3 orders of magnitude as λ increases over the range 0.0–0.2 m ($z_0 = 1.0 \times 10^{-4}$ to 1.0×10^{-2} m, u_{*t} = 0.2–0.8 m s^{-1}) [*Lancaster and Baas*, 1998; *Vest et al.*, 2013]. Calculating z_0 (and therefore u_*) from λ can be problematic and can thus result in highly abnormal flux estimates when applied with u_{*t} scaled by either measured or modeled drag partitions.

Removing all sources of variability due to roughness configuration from the *Raupach et al.* [1993] model reveals more about the reliability of the approach for predicting R'' effects on sediment flux (Figure 10). When the m and β_r parameters were held constant across the range of λ (i.e., as originally envisioned by *Raupach et al.* [1993]), modeled Q shows no difference between the roughness configurations, while flux estimates based on the measured τ''_S (Figure 6) indicate that differences should exist. This result confirms the inability of the *Raupach et al.* [1993] model to resolve the important effects of roughness configuration unless the m and β_r parameters are tuned for each configuration. As with our assessment of Q with variable m and β_r (Figure 9), we found that Q increases rather than declines with estimates of z_0 derived from λ [after *Marticorena et al.*, 1997, 2006].

4. Discussion and Conclusions

Taking a closer look at the results of *Brown et al.* [2008] suggests that the spatial distribution of roughness elements has a significant effect on aeolian sediment flux. Roughness configuration moderates where sediment flux occurs in a landscape and the magnitude of the total flux within an eroding area. Our results show that the total flux predicted from measured τ'_S distributions [*Brown et al.*, 2008] can vary by more than 1 order of magnitude depending on roughness configuration (Figure 3).

©2014. American Geophysical Union. All Rights Reserved.

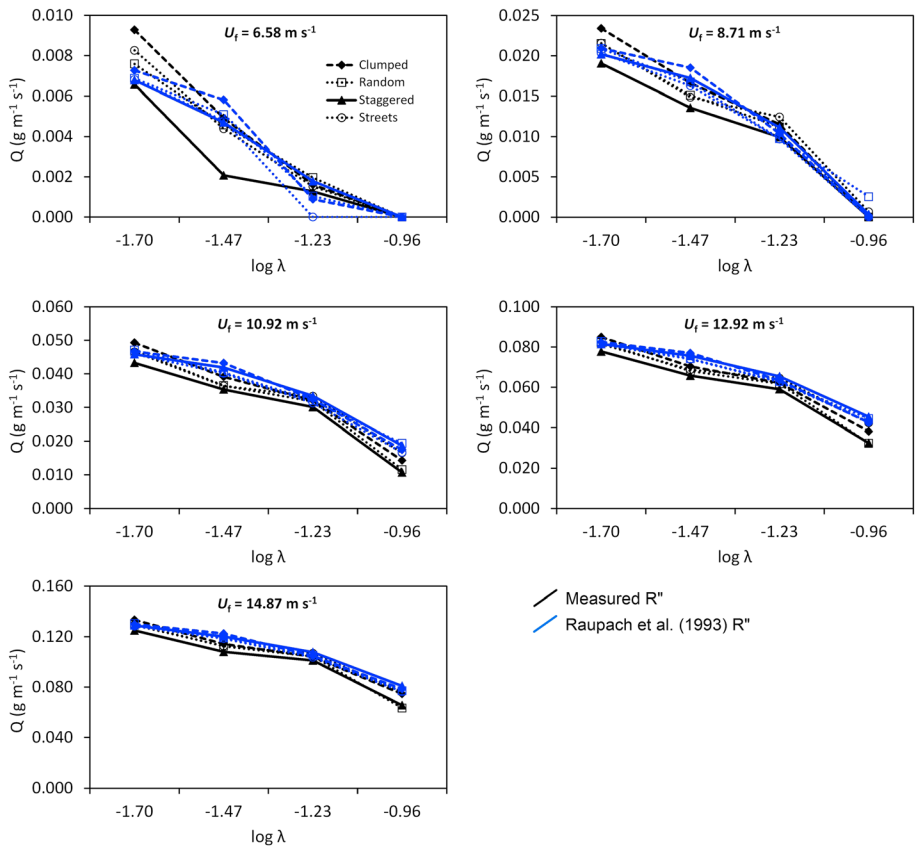

Figure 8. Plots of horizontal sediment mass flux Q (g m^{-1} s^{-1}) calculated from the measured and modeled [after *Raupach et al.*, 1993] R'' for the set of four roughness configurations at a range of λ and freestream wind velocities (U_f). Initial u_{*t} set to 0.25 m s^{-1}. Estimates of u_* as input to Q were based on constant z_0 (4×10^{-3} m), taken as the mean of z_0 measured in the wind tunnel experiments.

Roughness configuration can impact sediment flux by influencing the magnitude and distribution of shear stress over a surface that is in excess of the soil entrainment threshold. Roughness configuration matters most when the distribution of τ_S is close to the threshold for entrainment. It matters least when τ_S (u_*) $>> u_{*t}$, and at small roughness densities (Figure 3). If two roughness configurations produce different u_* distributions in excess of u_{*t}, their resulting sediment fluxes will be different. If the u_* distributions from two roughness configurations are alike, their resultant fluxes will be similar. Different roughness configurations may also produce the same sediment flux if the net effect of the total shear stress above the entrainment threshold is the same, despite the τ_S distributions being different. We posit that this latter case occurs when the wind energy incident on a surface is much greater than u_{*t} (Figure 3). Logically, roughness configuration has no effect on sediment flux when the distribution of τ_S (u_*) over a surface is below u_{*t}.

The influence of roughness configuration on sediment flux exists even when a distribution of wind speed is considered (Figure 4). This is because roughness configuration matters most when the distribution of τ_S is close to the threshold for soil entrainment. In a typical distribution, the wind shear velocity is much more likely to be close to the entrainment threshold than significantly above it. Therefore, although the effect of roughness distribution does not matter equally for all wind speeds, it will matter for the case of variable wind speed as observed routinely in field conditions.

Bulk drag partitioning schemes provide a practical means for representing surface roughness effects on aeolian sediment transport. Nonetheless, the approach consists of a conceptual simplification that is a considerable source of uncertainty. Bulk drag partitioning schemes assume that the threshold of particle movement is determined by τ''_s acting at any point on the surface [*Raupach et al.*, 1993]. Threshold is assumed to be exceeded everywhere at this maximum, producing uniform large sediment flux. Our results

©2014. American Geophysical Union. All Rights Reserved.

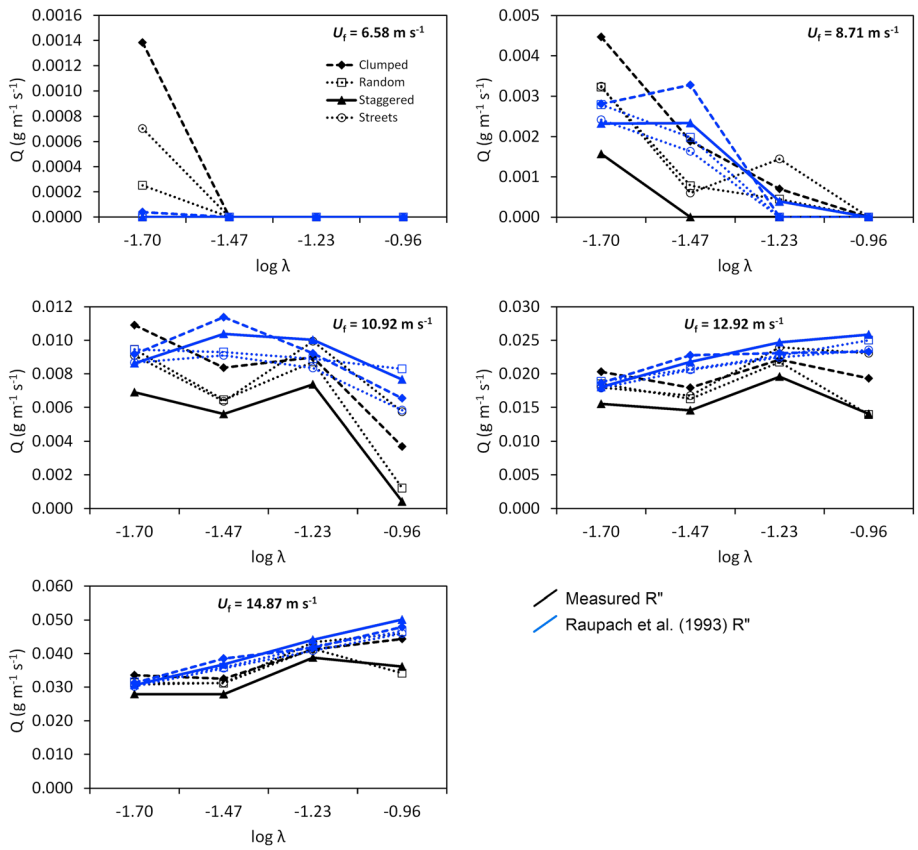

Figure 9. Plots of horizontal sediment mass flux Q (g m^{-1} s^{-1}) calculated from the measured and modeled [after *Raupach et al.*, 1993] R'' for the set of four roughness configurations at a range of λ and freestream wind velocities (U_f). Initial u_{*t} set to 0.25 m s^{-1}. Estimates of u_* as input to Q were based on z_0 calculated as a product of λ following *Marticorena et al.* [2006].

show that using a bulk drag partition coefficient to scale the threshold for soil entrainment (u_{*t}) can result in an overestimate of sediment flux by 2 to 3 orders of magnitude (Figures 6 and 7). Explicitly accounting for spatial variability in τ_S due to vegetation distribution better captures the magnitude and variability in sediment flux over vegetated landscapes [*Li et al.*, 2013; *Vest et al.*, 2013].

Interestingly, τ''_S (and therefore R'') appears to have some sensitivity to roughness configuration (Figure 5). While *Brown et al.* [2008] concluded that roughness configuration effects on R'' are small, our results show that these small differences have an important effect on Q. Using the drag partitioning approach to scale u_{*t} should, therefore, capture some of the effects of roughness configuration that influence sediment flux (Figure 6). Nonetheless, our results have confirmed that without tuning the *Raupach et al.* [1993] model m and β_r parameters for different roughness configurations, the model cannot represent expected variations in Q due to roughness configuration [*Crawley and Nickling*, 2003; *Walter et al.*, 2012a]. This limits the ability of the model to resolve variations in sediment flux due to vegetation distribution.

While β_r will vary depending on the characteristics of roughness elements (e.g., geometry), the practice of tuning β_r for different roughness densities (and configurations) presents additional problems. By definition, β_r should be insensitive to roughness density and configuration, though not necessarily wind speed because drag coefficients vary with Reynolds number. It is possible that β_r could vary with Reynolds number if the drag coefficient for elements embedded within a roughness array were to behave differently to that of isolated elements, but this has not been demonstrated. We consider the practice of tuning the β_r parameter to obtain a good fit of the drag partition model R'' with experimental data to be inconsistent with the theory of *Raupach et al.* [1993]. Whether the *Raupach et al.* [1993] model can resolve roughness configuration effects on R'' appears moot in light of the apparent larger uncertainty in estimating flux as a product of τ''_S

©2014. American Geophysical Union. All Rights Reserved.

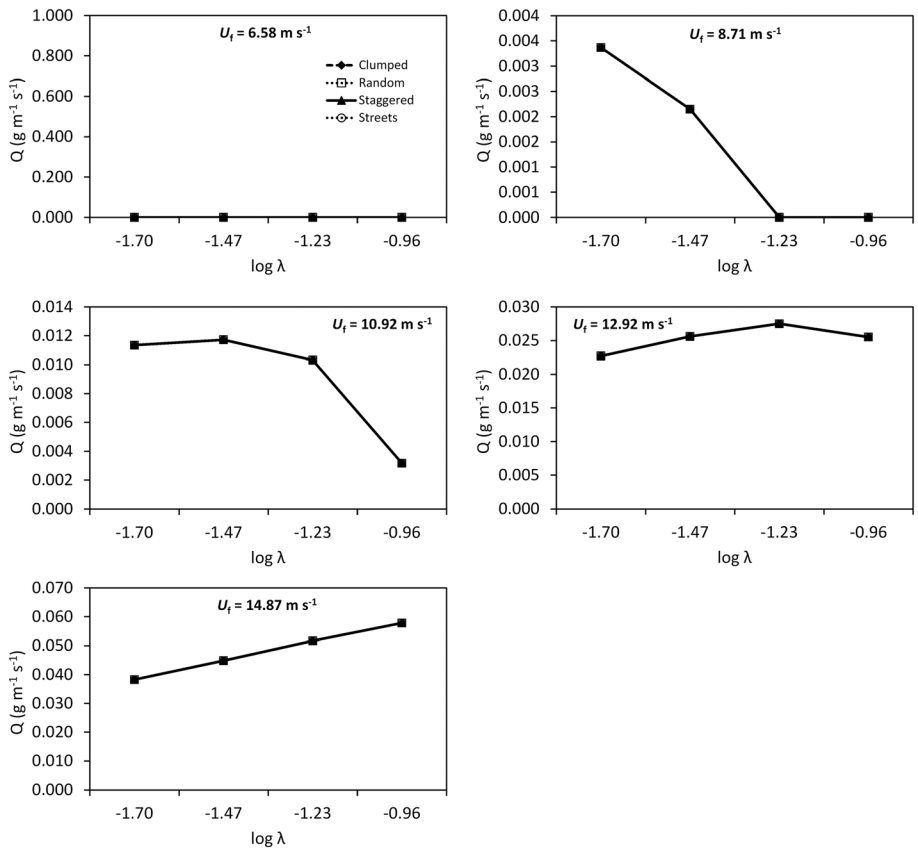

Figure 10. Plots of horizontal sediment mass flux Q (g m^{-1} s^{-1}) calculated from the modeled [after *Raupach et al.*, 1993] R'' for the set of four roughness configurations at a range of λ and freestream wind velocities (U_f). Initial u_{*t} set to 0.25 m s^{-1}. Here, input parameters m and β_r were held constant, as applied in *Shao et al.* [1994] to estimate R'' so that all roughness configuration effects were removed. Estimates of u_* were then disconnected from R'' by deriving z_0 from λ, following *Marticorena et al.* [2006].

over the land surface. Focusing on the distribution of τ_S makes the conceptual simplifications of this theory unnecessary and therefore also obviates the need to vary a constant parameter.

A final complication in applying bulk drag partitioning models to estimate aeolian transport is the need to match changes in R'' due to λ and roughness configuration with commensurate changes in z_0 that underpin u_*. Our estimates of Q using u_* calculated from measured and modeled z_0 [after *Marticorena et al.*, 1997, 2006] resulted in increases in Q with increasing roughness density (Figures 7 and 9). In the case of the measured values of z_0, differences due to roughness configuration resulted as well. However, monotonic declines in Q were expected to occur [*Lancaster and Baas*, 1998]. Increasing λ should increase u_{*t} at a rate greater than roughness increases u_*, such that at large roughness densities Q will decline. If estimates of z_0 do not result in appropriate changes in u_* for the given R'', then u_* may vary and be greater than u_{*t} at increasing roughness densities, thus producing unrealistic patterns of sediment flux.

The implication of this finding is that if bulk drag partitioning schemes are applied to estimate aeolian sediment transport, then care must be taken to accurately derive z_0 to estimate u_*. This is especially the case for regional-scale assessments, which typically use wind shear velocity data from atmospheric models. Our results suggest that if the aerodynamic roughness used to calculate u_* in atmospheric models is not consistent with the aeolian roughness height implicit in R'', estimates of horizontal and vertical sediment fluxes may become physically implausible. This link between z_0 and R'' in the application of drag partitioning schemes has been acknowledged previously [*Darmenova et al.*, 2009]. *Shao and Yang* [2008] demonstrated numerically that z_0 varies with λ to a maximum ($\lambda \approx 0.2$) then decreases with λ to z_0 of the bare surface. Thus,

©2014. American Geophysical Union. All Rights Reserved.

implementing the drag partition model requires that profiles of the mean wind and turbulence (i.e., z_0) must be known for a given λ and roughness configuration [*Shao and Yang*, 2008].

We have examined one approach to resolving the issue by estimating z_0 from λ following *Marticorena et al*. [1997, 2006]. Our findings suggest that there exists some internal inconsistency in using this approach with the *Raupach et al*. [1993] drag partitioning scheme, though at present we remain uncertain as to the nature of this conflict. A potential solution is to use wind speed data from above the turbulent boundary layer with the aeolian roughness height implicit in R'' (measured for the same land surface) to estimate u_* [*Darmenova et al*., 2009]. Developing reliable estimates of z_0 for a range of environments will be important for models that employ bulk drag partitioning schemes in vegetated drylands. Nevertheless, this approach will not alleviate the remaining uncertainties in the application of the drag partition model itself.

Representing the effects of roughness elements on near-surface aerodynamics is central to predicting patterns of wind erosion and dust emission. Few studies have sought to quantify the accuracy of aeolian transport models in vegetated dryland environments [*Li et al*., 2013], and the magnitude of error in estimates of national and global dust budgets remains largely unknown [*Shao et al*., 2011]. Our results support field studies of the effects of surface roughness on patterns of wind erosion [*Gillette*, 1999; *Okin and Gillette*, 2001; *Li et al*., 2013]. They show that accounting for the distribution of surface roughness could improve the accuracy of aeolian transport models over those that employ bulk drag partitioning schemes. Aeolian sediment transport over vegetated landscapes could be as much as 2 to 3 orders of magnitude smaller than previously identified with bulk drag partitioning approaches [*Shao et al*., 2011]. These results should make us question and re-evaluate current understanding of the magnitude of dust emissions from vegetated drylands and its impact on Earth-system processes.

While the accuracy of aeolian transport models may be improved by incorporating the effects of roughness configuration, operationalizing such approaches is a challenge for broad-scale modeling. However, unlike λ, the fractional cover of vegetation, vegetation height, and the spatial distribution of canopy interspaces can be easily measured in the field and used as input to aeolian transport models [*Vest et al*., 2013; *Webb et al*., 2014]. *McGlynn and Okin* [2006] developed an approach for characterizing the distribution of shrubs in a desert landscape using high spatial resolution (1 m) remote sensing. While there is a significant gap in scale, such approaches give promise to the development of methods for quantifying the spatial distribution of vegetation at moderate resolutions (e.g., 500 m) with global application potential. For example, the spatial distribution of vegetation indices (e.g., normalized difference vegetation index and cellulose absorption index) derived from Moderate Resolution Imaging Spectroradiometer could be used as a proxy for estimating roughness distributions at coarse ($>$5 km) spatial resolutions following the concepts of *McGlynn and Okin* [2006]. Field measurements of fractional vegetation cover and the distribution of vegetation canopy gaps could also be used to derive lookup tables from which roughness distribution could be applied in regional-scale model applications. Even without knowledge of the exact spatial distribution of plants, assuming a Gaussian distribution of cover within vegetated areas would likely account for roughness effects and reduce uncertainty over estimates derived with the bulk partitioning approach using the λ parameter [*Okin*, 2008].

Given the scale-dependent nature of λ, increasing the spatial resolution of inputs to drag partitioning models may yield some improvement in their capacity to resolve spatial heterogeneity in aeolian transport. Nonetheless, the marginal gains from increased data resolution are unlikely to account for the significant overprediction of sediment flux modeled as a product of R''. Explicitly representing the spatial distribution of surface roughness on τ_S [e.g., *Okin*, 2008] will reduce uncertainty in estimates of wind erosion and dust emission from vegetated landscapes. Accounting for spatiotemporal variations in u_{*t} [*Webb and Strong*, 2011], the inhomogeneous availability of erodible sediment [*Gillies et al*., 2014], and the interacting effects of large roughness elements on sediment transport efficiency [*Gillies and Lancaster*, 2012] are additional challenges with potentially large impacts for modeling aeolian sediment transport. Projected global climate and land use changes will continue to modify vegetation cover, structures, and distributions in dryland environments [*Sivakumar*, 2007]. Models that can explicitly represent these changes in vegetation will provide the best opportunities for assessing the consequences for soil erosion and land degradation, quantifying their impacts on Earth-system processes, and identifying practical management solutions.

©2014. American Geophysical Union. All Rights Reserved.

Notation

A	constant present in equation for Q [*Shao et al.*, 1993]
b	roughness element breadth, m
β_r	ratio of element to surface drag coefficients (C_R/C_S), dimensionless
C_R	drag coefficient of an individual roughness element, dimensionless
Cs	drag coefficient of the unobstructed surface, dimensionless
D	soil grain diameter, m
F	vertical sediment flux, g m^{-1} s^{-1}
g	acceleration due to gravity, m s^{-2}
h	roughness element height, m
$H(w)$	correction function for soil water content (w), dimensionless
k	von Kármán constant, 0.4
λ	roughness density or lateral cover
m	empirical parameter [*Raupach et al.*, 1993]
n	number of roughness elements occupying the ground area of the roughness array
ρ_a	density of air, kg m^{-3}
Q	horizontal sediment flux, g m^{-2} s^{-1}
R	shear stress ratio, dimensionless
R''	maximum shear stress ratio, dimensionless
u_*	wind shear velocity, m s^{-1}
τ	total shear stress on the surface in the presence of roughness elements, N m^{-2}
τ_R	shear stress on roughness elements, N m^{-2}
τ_S	surface shear stress, N m^{-2}
τ'_S	average surface shear stress on the area not covered by roughness elements, N m^{-2}
τ''_S	maximum surface shear stress on the area not covered by roughness elements, N m^{-2}
φ	drag force on individual roughness element, N m^{-2}
σ_r	basal to frontal area ratio of roughness elements, dimensionless
u_{*t}	threshold wind shear velocity, m s^{-1}
u_{*ts}	threshold wind shear velocity of bare surface, m s^{-1}
U_f	freestream wind velocity, m s^{-1}
U_z	wind velocity at height z (m), m s^{-1}
z	height above ground surface, m
z_0	aerodynamic roughness height, m

Acknowledgments
We thank W.G. Nickling and J.A. Gillies for their contributions to the wind tunnel experiments and manuscript review. We also thank the two anonymous reviewers for their constructive comments on the manuscript. This work was supported by the Jornada Basin LTER (NSF DEB 12358218) and NSF grant EAR-1148334.

References

Brown, S., W. G. Nickling, and J. A. Gillies (2008), A wind tunnel examination of shear stress partitioning for an assortment of surface roughness distributions, *J. Geophys. Res.*, *113*, F02S06, doi:10.1029/2007JF000790.

Crawley, D. M., and W. G. Nickling (2003), Drag partitioning for regularly-arrayed rough surfaces, *Boundary Layer Meteorol.*, *107*, 445–468.

Darmenova, K., I. N. Sokolik, Y. Shao, B. Marticorena, and G. Bergametti (2009), Development of a physically based dust emission module within the Weather Research and Forecasting (WRF) model: Assessment of dust emission parameterizations and input parameters for source regions in central and East Asia, *J. Geophys. Res.*, *114*, D14201, doi:10.1029/2008JD011236.

Dong, Z., S. Gao, and D. W. Fryrear (2001), Drag coefficients, roughness length and zero-plane displacement height as disturbed by artificial standing vegetation, *J. Arid Environ.*, *49*, 485–505.

Dupont, S., G. Bergametti, and S. Simoëns (2014), Modeling aeolian erosion in presence of vegetation, *J. Geophys. Res. Earth Surf.*, *119*, 168–187, doi:10.1002/2013JF002875.

Gillette, D. A. (1999), A qualitative geophysical explanation for "Hot Spot" dust emitting source regions, *Contrib. Atmos. Phys.*, *72*, 67–77.

Gillette, D. A., and R. Passi (1988), Modeling dust emission caused by wind erosion, *J. Geophys. Res.*, *93*(D11), 14,233–14,242.

Gillette, D. A., and P. H. Stockton (1989), The effect of nonerodible particles on wind erosion of erodible surfaces, *J. Geophys. Res.*, *94*, 12,885–812,893.

Gillette, D. A., J. Adams, A. Endo, D. Smith, and R. Kihl (1980), Threshold velocities for input of soil particles into the air by desert soils, *J. Geophys. Res.*, *85*, 5621–5630.

Gillette, D. A., J. E. Herrick, and G. Herbert (2006), Wind characteristics of mesquite streets in the northern Chihuahuan Desert, New Mexico, U.S.A., *Environ. Fluid Mech.*, *6*, 241–275.

Gillies, J. A., and N. Lancaster (2012), Large roughness element effects on sand transport, Oceano Dunes, California, *Earth Surf. Processes Landforms*, *38*, 785–792.

©2014. American Geophysical Union. All Rights Reserved.

Gillies, J. A., N. Lancaster, W. G. Nickling, and D. M. Crawley (2000), Field determination of drag forces and shear stress partitioning effects for a desert shrub (*sarcobatus vermiculatus*, greasewood), *J. Geophys. Res.*, *105*(D20), 24,871–24,880.
Gillies, J. A., W. G. Nickling, and J. King (2007), Shear stress partitioning in large patches of roughness in the atmospheric inertial sublayer, *Boundary Layer Meteorol.*, *122*, 367–396.
Gillies, J. A., J. M. Nield, and W. G. Nickling (2014), Wind speed and sediment transport recovery in the lee of a vegetated and denuded nebkha within a nebkha dune field, *Aeolian Res.*, *12*, 135–141.
Irwin, H. P. A. H. (1980), A simple omnidirectional sensor for wind-tunnel studies of pedestrian level winds, *J. Wind Eng. Industrial Aerodynamics*, *7*, 219–239.
King, J., W. G. Nickling, and J. A. Gillies (2006), Aeolian shear stress ratio measurements within mesquite-dominated landscapes of the Chihuahuan Desert, New Mexico, U.S.A., *Geomorphology*, *82*, 229–244.
Lancaster, N., and A. Baas (1998), Influence of vegetation cover on sand transport by wind: Field studies at Owens Lake, California, *Earth Surf. Processes Landforms*, *23*, 69–82.
Li, J., G. S. Okin, J. E. Herrick, J. Belnap, S. M. Munson, M. E. Miller, K. R. Vest, and A. E. Draut (2013), Evaluation of a new model of aeolian transport in the presence of vegetation, *J. Geophys. Res. Earth Surf.*, *118*, 288–306, doi:10.1002/jgrf.20040.
Luttmer, C. (2002), The partition of drag in salt grass communities, Masters' thesis submitted to The Univ. of Guelph, 138 pp.
Marshall, J. K. (1971), Drag measurements in roughness arrays of varying density and distribution, *Agric. Meteorol.*, *8*, 269–292.
Marshall, J. K. (1972), Principles of soil erosion and its prevention, in *The use of Trees and Shrubs in the Dry Country of Australia*, edited by N. Hall et al., pp. 90–107, Dep. of Natl. Dev., For. and Timber Bur. Aust. Govt. Pub. Serv., Canberra.
Marticorena, B., and G. Bergametti (1995), Modeling the atmospheric dust cycle: 1. Design of a soil-derived dust emission scheme, *J. Geophys. Res.*, *100*(D8), 16,415–416,430.
Marticorena, B., G. Bergametti, B. Aumont, Y. Callot, C. N'Doumé, and M. Legrand (1997), Modeling the atmospheric dust cycle 2. Simulation of Saharan dust sources, *J. Geophys. Res.*, *102*(D4), 4387–4404.
Marticorena, B., et al. (2006), Surface and aerodynamic roughness in arid and semiarid areas and their relation to radar backscatter coefficient, *J. Geophys. Res.*, *111*, F03017, doi:10.1029/2006JF000462.
McGlynn, I. O., and G. S. Okin (2006), Characterization of shrub distribution using high spatial resolution remote sensing: Ecosystem implications for a former Chihuahuan Desert grassland, *Remote Sens. Environ.*, *101*, 554–566.
Okin, G. S. (2008), A new model of wind erosion in the presence of vegetation, *J. Geophys. Res.*, *113*, F02S10, doi:10.1029/2007JF000758.
Okin, G. S., and D. A. Gillette (2001), Distribution of vegetation in wind-dominated landscapes: Implications for wind erosion modelling and landscape processes, *J. Geophys. Res.*, *106*(D9), 9673–9683.
Panofsky, H. A., and D. A. Dutton (1984), *Atmospheric Turbulence*: *Models and Methods for Engineering Applications*, 397 pp., John Wiley, Hoboken, N.J.
Raupach, M. R. (1992), Drag and drag partitioning on rough surfaces, *Boundary Layer Meteorol.*, *60*(4), 375–395.
Raupach, M. R., and H. Lu (2004), Representation of land-surface processes in aeolian transport models, *Environ. Modell. Software*, *19*(2), 93–112.
Raupach, M. R., D. A. Gillette, and J. F. Leys (1993), The effect of roughness elements on wind erosion threshold, *J. Geophys. Res.*, *98*(D2), 3023–3029.
Ravi, S., et al. (2011), Aeolian processes and the biosphere, *Rev. Geophys.*, *49*, RG3001, doi:10.1029/2010RG000328.
Shao, Y., M. R. Raupach, and P. A. Findlater (1993), Effect of saltation bombardment on the entrainment of dust by wind, *J. Geophys. Res.*, *98*(D7), 12,719–12,726.
Shao, Y., R. M. Raupach, and D. Short (1994), Preliminary assessment of wind erosion patterns in the Murray-Darling Basin, *Aust. J. Soil Water Conserv.*, *7*(3), 46–51.
Shao, Y. (2008), *Physics and Modelling of Wind Erosion*, 393 pp., Kluwer Acad., London.
Shao, Y., and Y. Yang (2008), A theory for drag partition over rough surfaces, *J. Geophys. Res.*, *113*, F02S05, doi:10.1029/2007JF000791.
Shao, Y., K.-H. Wyrwoll, A. Chappell, J. Huang, Z. Lin, G. H. McTainsh, M. Mikami, T. Y. Tanaka, X. Wang, and S. Yoon (2011), Dust cycle: An emerging core theme in Earth system science, *Aeolian Res.*, *2*, 181–204.
Sivakumar, M. V. K. (2007), Interactions between climate and desertification, *Agric. For. Meteorol.*, *142*, 143–155.
Sorensen, M. (1991), An analytical model of windblown sand transport, in *Aeolian Grain Transport: Mechanics*, Acta Mechanica Supplement 1, edited by O. E. Barndorff-Nielson and B. B. Willetts, pp. 67–81, Springer, Dordrecht.
Vest, K. R., A. J. Elmore, J. M. Kaste, G. S. Okin, and J. Li (2013), Estimating total horizontal aeolian flux within shrub-invaded groundwater dependent meadows using empirical and mechanistic models, *J. Geophys. Res. Earth Surf.*, *118*, 1132–1146, doi:10.1002/jgrf.20048.
von Kármán, T. (1934), Turbulence and skin friction, *J. Aeronautical Sci.*, *1*, 1–20.
Walter, B., C. Gromke, and M. Lehning (2012a), Shear-stress partitioning in live plant canopies and modifications to Raupach's model, *Boundary Layer Meteorol.*, *144*, 217–241.
Walter, B., C. Gromke, K. C. Leonard, C. Manes, and M. Lehning (2012b), Spatio-temporal surface shear-stress variability in live plant canopies and cube arrays, *Boundary Layer Meteorol.*, *143*, 337–356.
Webb, N. P., and H. A. McGowan (2009), Approaches to modelling land erodibility by wind, *Prog. Phys. Geogr.*, *33*(5), 587–613.
Webb, N. P., and C. L. Strong (2011), Soil erodibility dynamics and its representation for wind erosion and dust emission models, *Aeolian Res.*, *3*, 165–179.
Webb, N. P., J. E. Herrick, and M. C. Duniway (2014), Ecological site-based assessments of wind and water erosion: Informing accelerated soil erosion management in rangelands, *Ecol. Appl.*, doi:10.1890/13-1175.1, in press.
Wolfe, S. A., and W. G. Nickling (1996), Shear stress partitioning in sparsely vegetated desert canopies, *Earth Surf. Processes Landforms*, *21*, 607–619.

©2014. American Geophysical Union. All Rights Reserved.